NeuroImage 117 (2015) 343–357

Contents lists available at ScienceDirect

NeuroImage

journal homepage: www.elsevier.com/locate/ynimg

An automated pipeline for constructing personalized virtual brains from multimodal neuroimaging data

Michael Schirner [a,b,1], Simon Rothmeier [a,b,1], Viktor K. Jirsa [c], Anthony Randal McIntosh [d], Petra Ritter [a,b,e,f,*]

[a] Dept. Neurology, Charité — University Medicine, Berlin, Germany
[b] Bernstein Focus State Dependencies of Learning, Bernstein Center for Computational Neuroscience, Berlin, Germany
[c] Institut de Neurosciences des Systèmes UMR INSERM 1106, Aix-Marseille Université Faculté de Médecine, Marseille, France
[d] Rotman Research Institute of Baycrest Centre, University of Toronto, Toronto, Canada
[e] Minerva Research Group BrainModes, Max Planck Institute for Human Cognitive and Brain Sciences, Leipzig, Germany
[f] Berlin School of Mind and Brain, Mind and Brain Institute, Humboldt University, Berlin, Germany

ARTICLE INFO

Article history:
Received 27 October 2014
Accepted 19 March 2015
Available online 31 March 2015

Keywords:
The Virtual Brain
Connectome
Tractography
Diffusion MRI
Multimodal imaging
Computational modeling

ABSTRACT

Large amounts of multimodal neuroimaging data are acquired every year worldwide. In order to extract high-dimensional information for computational neuroscience applications standardized data fusion and efficient reduction into integrative data structures are required. Such self-consistent multimodal data sets can be used for computational brain modeling to constrain models with individual measurable features of the brain, such as done with The Virtual Brain (TVB). TVB is a simulation platform that uses empirical structural and functional data to build full brain models of individual humans. For convenient model construction, we developed a processing pipeline for structural, functional and diffusion-weighted magnetic resonance imaging (MRI) and optionally electroencephalography (EEG) data. The pipeline combines several state-of-the-art neuroinformatics tools to generate subject-specific cortical and subcortical parcellations, surface-tessellations, structural and functional connectomes, lead field matrices, electrical source activity estimates and region-wise aggregated blood oxygen level dependent (BOLD) functional MRI (fMRI) time-series. The output files of the pipeline can be directly uploaded to TVB to create and simulate individualized large-scale network models that incorporate intra- and intercortical interaction on the basis of cortical surface triangulations and white matter tractography. We detail the pitfalls of the individual processing streams and discuss ways of validation. With the pipeline we also introduce novel ways of estimating the transmission strengths of fiber tracts in whole-brain structural connectivity (SC) networks and compare the outcomes of different tractography or parcellation approaches. We tested the functionality of the pipeline on 50 multimodal data sets. In order to quantify the robustness of the connectome extraction part of the pipeline we computed several metrics that quantify its rescan reliability and compared them to other tractography approaches. Together with the pipeline we present several principles to guide future efforts to standardize brain model construction. The code of the pipeline and the fully processed data sets are made available to the public via The Virtual Brain website (thevirtualbrain.org) and via github (https://github.com/BrainModes/TVB-empirical-data-pipeline). Furthermore, the pipeline can be directly used with High Performance Computing (HPC) resources on the Neuroscience Gateway Portal (http://www.nsgportal.org) through a convenient web-interface.

Introduction

In biology, the notion that structure predicts function is widespread. In human neurosciences, different modalities image different structural aspects making their integration imperative to predict function (Sporns, 2013). The Virtual Brain (TVB, thevirtualbrain.org) uses empirical structural and functional data to build full brain models of individual primates—consisting of interacting dynamic local models—that predict individual whole-brain activity on different scales (Ritter et al., 2013; Sanz-Leon et al., 2013; Roy et al., 2014; Woodman et al., 2014). The interactions between neuronal populations in a full brain model are constrained by the anatomical fiber skeleton, i.e., the structural connectome, obtained from diffusion-weighted magnetic resonance imaging (dwMRI) using tractography techniques. The human brain connectome is the set of neuronal connections in the human brain, a concept that crosses spatial brain scales (Sporns et al., 2005; Craddock

* Corresponding author at: Max Planck Institute for Human Cognitive and Brain Sciences Leipzig, Department of Neurology, Charité Universitaetsmedizin, Charitéplatz 1, 10117 Berlin, Germany. Fax: +49 30 450 560 936.
E-mail address: petra.ritter@charite.de (P. Ritter).
[1] Equal contributions.

http://dx.doi.org/10.1016/j.neuroimage.2015.03.055

et al., 2013). The term connectome is used in the literature for functional connectivity (FC; i.e., statistical dependencies of brain activity), structural connectivity (SC; i.e., anatomical connections between brain areas) and effective connectivity (EC; i.e., causal interaction between brain areas). A connectome is often represented as a weighted graph with nodes defining brain regions and edges characterizing the connections between these regions. FC is a highly variable and non-stationary activity pattern (Bassett et al., 2011b; Allen et al., 2014; Hutchison et al., 2013; Zalesky et al., 2014) arising from interactions within the structural skeleton. FC is a statistical concept that estimates correlations between data from simultaneous measurements of different brain areas that does not necessarily reflect the neuroanatomical structures. On the other hand, the anatomical connection pattern or wiring diagram between neurons and neuronal ensembles, dubbed SC, is typically described in terms of distances and connection strengths mediated by synaptic or electric connections between region pairs. In contrast, EC captures the causal relations between neural systems by quantifying the directed influences that one element of a generative model exerts over another (Valdes-Sosa et al., 2011).

In recent years, efforts for multicenter data sharing have increased and several large-scale projects started to collaboratively pool and compile multimodal neuroimaging data, e.g., (Biswal et al., 2010; Van Essen et al., 2012). The Neuroscience Information Framework (http://neuinfo.org/) lists over 2500 different databases with relevance for neuroscience. This high number of heterogeneous resources requires standardized and efficient processing routines in order to (i) extract interpretable and relevant information and to (ii) organize and integrate it in a systematic and unifying structure: "Perhaps the single biggest roadblock to higher order data mining is the lack of standardized frameworks for organizing neuroscience data" (Akil et al., 2011).

We propose to go one step further: In order to get from pure data gathering to knowledge inference we need to connect functional and structural data by means of model-based integration (Jirsa et al., 2002, 2010; Ritter et al., 2013). The formulation of a comprehensive theory of neural computation that allows a qualitative and quantitative mapping between cognitive and neural states is only possible if we close the loop between data-driven inference and model-based prediction. Jirsa et al. (2002) merged geometric and topographic structural information with brain network modeling, but used simplified network connectivity and demonstrated that temporal activation patterns are well captured as observed in human brain imaging. A necessary condition to produce realistic spatiotemporal activations is the additional inclusion of topological information, that is, realistic network connectivity, which poses substantial neuroinformatics challenges. The Virtual Brain is a step into this direction and provides an integrated neuroinformatics platform (Sanz-Leon et al., 2013) for modeling dynamic large-scale brain network models (BNM) constructed from structural data and interacting local dynamic population models. Within its theoretical framework, TVB integrates the relevant information extracted from a variety of empirical sources associating brain network structure with brain function via models of neural activity. By doing so, it abstracts from the high dimensionality of information contained in raw imaging data and unifies relevant structural and dynamical information within a single brain model. The unified theoretical framework provided by TVB together with the processing pipeline for multimodal empirical data opens up new avenues of collective neuroscience. TVB empowers the community to conveniently construct biologically informed brain models, to perform in silico experiments that predict neuronal activity and to expose principles of computation across spatial and temporal scales in a variety of modalities.

Data reduction and fusion are prerequisites for automated data analysis, to ensure interoperability of data structures and for comparability of multicenter acquisitions. One example is the alignment of the spatial and temporal dimensions of recordings from different modalities within and across subjects and their integration into a common reference system. Data turns into information when they are semantically annotated and ontologically aligned. Extracted information gains maximal interpretability when mappings between data sets and their organization into a unified coordinate system can be achieved, e.g., the registration and mapping of anatomical structures between modalities or temporal alignment of simultaneously acquired multimodal data (Calhoun and Lemieux, 2014; Jorge et al., 2014; James and Dasarathy, 2014; Uludağ and Roebroeck, 2014).

The processing pipeline presented in this article provides an efficient and automated way for generating full and self-consistent data sets for TVB model construction integrating anatomical, diffusion weighted and functional MRI scans with EEG recordings. Online supplementary Movie M1 illustrates the involved imaging modalities and estimated source activity along with brain network activity projected onto reconstructed head and cortex models of the exemplary subject QL used throughout this paper. The pipeline runs on standard computers, but also supports a high degree of parallelization for computationally intensive processes, optimized to run on stand-alone workstations and high performance clusters alike. In the following, we describe the functionality of the pipeline by demonstrating each step on the exemplary data set. Up to now we pre-processed 50 full data sets using this pipeline. All data sets were stored in the TVB XNAT (Marcus et al., 2007) database in Toronto where they are made available to the TVB consortium. Along with the processing steps, we illustrate the challenges posed when working with multimodal imaging data and integrating them in a single framework such as provided by TVB. These challenges range from storage requirements due to large amounts of data, interoperability and interfacing between different toolboxes and coordinate systems, fallacies of dwMRI tractography to outcome validation. Each of the imaging modalities serves different purposes during model generation and optimization within TVB:

(i) High resolution *T1-weighted MRI* scans are used to obtain parcellations of cortical and subcortical white and gray matter (WM, GM) into subregions of interest based on anatomical landmarks and to construct anatomically constrained dipole source models for forward modeling and inverse source reconstruction of EEG and magnetoencephalography (MEG). Resulting lead-field matrices and inversion kernels are used to map cortical activity to scalp locations of (M)EEG sensors and vice versa. Furthermore, high-resolution scalp/head, skull and cortex-surface triangulations are used for highly resolved surface simulations and output visualization.

(ii) *fMRI* volumes are parcellated according to the high-resolution atlases derived from T1-weighted data yielding region-wise aggregated BOLD time-series and FC matrices generated from these are used to fit model output by means of parameter tuning.

(iii) *Diffusion-weighted MRI (dwMRI)* data are parcellated according to the high-resolution atlases derived from T1-weighted data yielding estimated white matter fiber tracts and SC matrices. The parcellations are used for defining seed- and stop-locations during tractography.

(iv) *EEG* data is projected to source space and used to optimize parameters of the brain model.

Pipeline results are provided in a format that can be directly imported to TVB and readily integrated into a single full-brain model. As part of this pipeline a novel tractography-based connectome extraction approach is described. The method introduces several concepts that facilitate the standardization of the BNM construction process. Connectomes are embedded at the core of the generic BNM equation to define long-range information transmission thereby linking large-scale network infrastructure with neural mass dynamics. In this context, connectomes are based on a given parcellation of the brain and consist

of two matrices that describe the strength and the time-delay of signal transmission between each pair of brain regions. Coupling strengths and distances (that are turned into delays by dividing through transmission velocity) define the mutual interaction of nodes within the BNM equation, which states in its most general form that the evolution of activity of a certain node in the network is the sum of its intrinsic local dynamics (often described by a neural mass model), input from connected regions, external input, and a term that accounts for different types of noise (Sanz-Leon et al., 2015). Long-range input for a given population is computed by summing the scaled and delayed activity of connected nodes according to such strengths and time-delay matrices. BNMs are—similar to models used in dynamic causal modeling (Friston et al., 2003)—biophysical network models of coupled differential equations that describe the underlying neuronal dynamics of observed data. In contrast to DCM where typically only few regions are used (to enable Bayesian model inversion), BNMs attempt to model a whole brain network. Similar to DCM, the coupling parameters of BNMs that predict neural activity form a hypothesis about how one brain region exerts a directed influence upon another region, i.e. their effective connectivity.

An important criterion for the quality of extracted subject-specific models is the ability to infer physiologically relevant individual variation. In other words, the inferred inter-individual differences should outweigh estimation bias. One goal of connectome extraction is robustness, i.e., low intra-individual variability of structural connectomes extracted from different data sets of the same subject, while maintaining biological variability that gives rise to differential dynamics between different subjects. Metrics that estimate the rescan-variability of the pipeline show very high robustness and almost identical connectomes extracted from different scans of the same subjects (average intra-subject correlation $r = 0.98$), while maintaining between-subject inter-individual variability at the same time (average inter-subject correlation $r = 0.89$).

Apart from computational modeling, SC matrices are also analyzed with methods from graph theory to study the organization of the brain network and associate it with function (Hagmann et al., 2008; Bullmore and Sporns, 2009).

Preliminary partial least square analyses of resulting connectomes showed significant age-depended modulations of several network features (e.g., density of individual axonal tracts ($r = .82$, $p < .01$, 95% CI [0.77, .90]), strength of functional interactions between regions ($r = 0.54$, $p < .01$, 95% CI [0.53, 0.82]) (Zimmermann et al., 2014)).

The software can be installed from online repositories (https://github.com/BrainModes/TVB-empirical-data-pipeline or thevirtualbrain.org) or directly used with HPC resources on the Neuroscience Gateway Portal (http://www.nsgportal.org) through a convenient web-interface (Sivagnanam et al., 2013).

Methods and results

Multimodal data acquisition

In this study we analyze 49 resting state simultaneous EEG–fMRI data sets acquired at Berlin Center for Advanced Imaging, Charité University Medicine, Berlin, Germany (age ranged from 18 to 80 years, mean 41.55 ± 18.44; 30 females and 19 males) and one simultaneous EEG–fMRI data set under task conditions acquired at Baycrest Centre, Toronto, Canada (54 year old female). After EEG–fMRI acquisition, anatomical and diffusion weighted images of subjects were acquired. In order to characterize the test–retest robustness of the connectome estimation, an additional dataset of three subjects was acquired in Berlin consisting of anatomical and diffusion weighted scans. In this case, each subject was scanned three times; the first two scans were acquired in sequence without a break in between. For the third scan the subject was moved out of the scanner in order to modify head position and moved back into the scanner. The Berlin subjects were asked to keep awake and to keep the eyes closed — no other controlled task had to be performed. At Baycrest Centre, the subject was equipped with the EEG cap, moved into the MR scanner and localizer, anatomical T1 and four functional runs were performed. Then, upon removing the subject from the scanner and removing the EEG cap, the subject was moved back into the scanner and one localizer, dwMRI and T2 sequence were recorded. MR and EEG acquisition setup, parameters and EEG preprocessing can be found in the Supplementary material.

Pipeline workflow

In the following, we demonstrate the individual steps of the processing pipeline on one example data set (Fig. 1 and supplementary Movie M1) and evaluate its outputs. The results provide insights on the meaning and interpretability of various measures used in previous studies, e.g., metrics of structural or functional connectivity, and shall assist future users of the pipeline for selecting suitable outputs in the context of their study. A detailed overview of the pipeline workflow and the interaction of different software modules are shown in Supplementary Fig. 1. The average amount of processed and stored data generated by the pipeline is 89.9 ± 15.12 GB per subject, but depends on the properties of the data set (e.g., resolution of dwMRI data) and used pipeline settings (e.g., number of generated tracks). The inter-subject differences of data size and computation time for a data set with identical acquisition parameters are mainly explained by differences in brain size (connectome extraction depends on the number of seed voxels). All computations described in the following section were done on a high performance computer consisting of multicore CPUs at a clock rate of ~2.54 GHz per CPU core and 8GB RAM per core. In Table 1, we provide the generated data amount and computational cost of each individual step.

Under the assumption of linear scalability, we calculated execution time of the pipeline based on our test setup (computer consisting of 184 CPU cores at a clock-rate of 2.54 GHz). The scaling assumes an octa-core workstation with equally fast CPU cores and I/O latencies. Only the tractography and connectome extraction modules of the pipeline are parallelized. Since preprocessing steps are all executed on a single core their executional times are scale invariant. The accumulated execution time for these scale invariant preprocessing processes is around 10 h.

- Fiber Tractography: around 2 h. Hence for a work station as described above: (2 h * 184 Cores)/8 Cores = 46 h.
- Computing SC Matrices: 2 h using a maximum of 68 cores in parallel. For a workstation hence it follows: (2 h * 68 cores)/8 cores = 17 h.

To process a single subject from the raw DICOM data to the final SC & FC matrices using a workstation containing eight CPU cores, one would need approximately 73 h.

Mandatory pipeline inputs are three raw MRI data sets in DICOM format: T1-weighted structural, BOLD and dwMRI with at least 45 distinct gradient directions and one b0 image as first image in the data set. Optionally, one EEGLAB set file and one data set containing axon tract directionality information, e.g., derived from CoCoMac database, http://cocomac.org, and adapted to the human brain (Bezgin et al., 2012) can be read. Exemplary pipeline output files compatible with TVB upload requirements are public and can be found via this URL: https://github.com/the-virtual-brain/tvb-data.

A detailed description of pipeline output, TVB file formats and the optional EEG source-imaging step can be found in the Supplementary material.

Preprocessing of T1-weighted anatomical MRI data

High-resolution anatomical images are used to create a segmentation of white matter, for segmentation and parcellation of cortical and

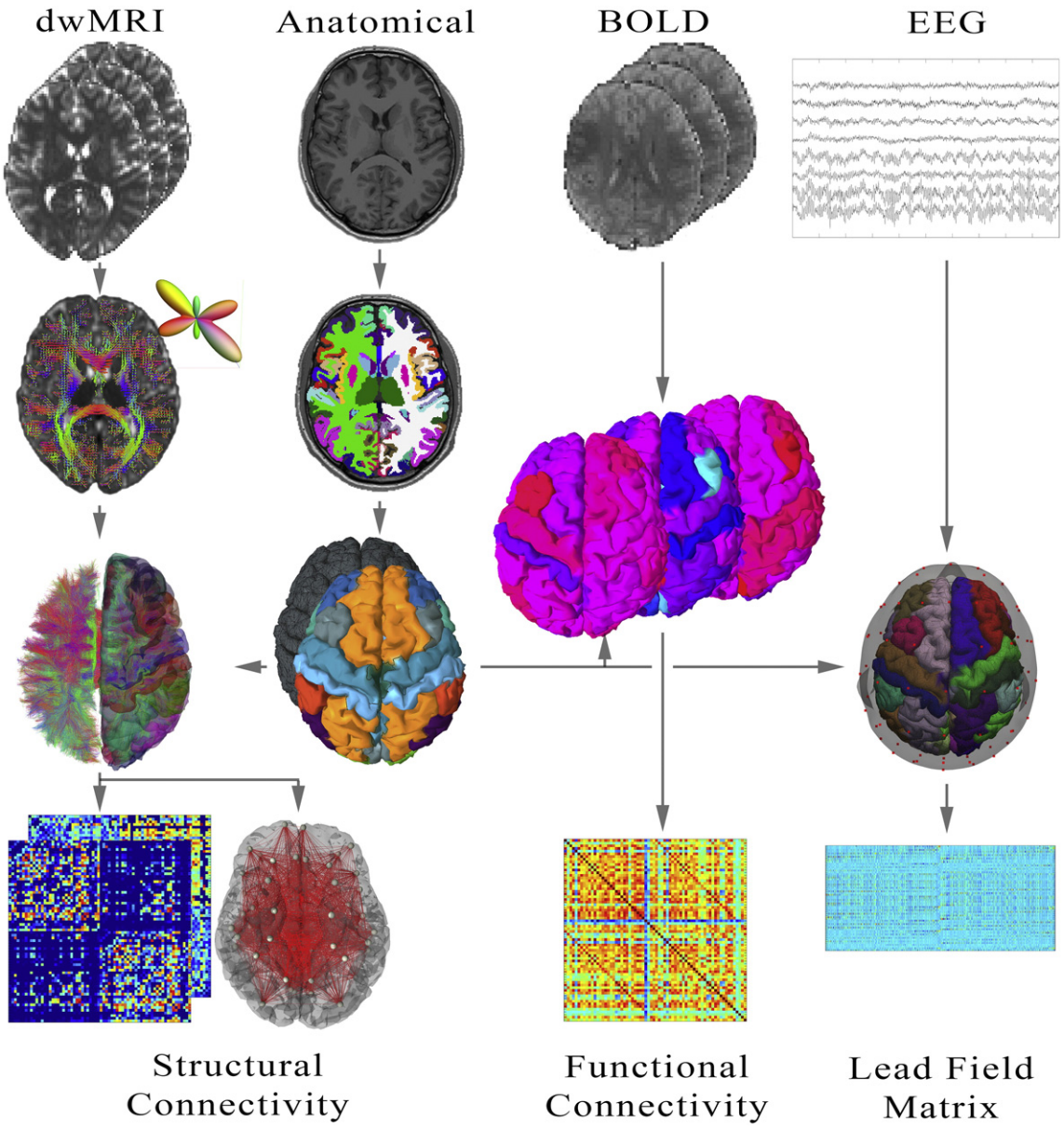

Fig. 1. Illustration of pipeline input and output based on imaging data of one subject. Input is anatomical, functional and diffusion MRI data. Optionally, EEG data can be inputted for source estimation. The output includes surface triangulations (scalp/head, skull, cortical), tracks returned by tractography, tracks aggregated to SC matrices, source activity, region-wise BOLD activity and FC matrices.

subcortical gray matter (to be used for full-brain simulation within TVB and for the extraction of region-wise averaged BOLD activity) and for the generation of tractography masks. The following major steps are performed by FREESURFER's *recon-all* function: motion correction, intensity normalization, skull stripping, removal of non-brain tissue, brain mask generation, cortical reconstruction, WM and subcortical segmentation, cortical tessellation generating GM–WM and GM-pia interface surface-triangulations and probabilistic atlas based cortical and subcortical parcellation. Relevant output of these operations are NifTi volumes that contain GM and WM parcellations.

Optional: Using parcellations defined for standard brain templates

Optionally, warping-based normalization of subject-specific brains to the MNI152 standard brain (Grabner et al., 2006) can be selected. Brain normalization by warping is an error prone procedure that often results in misalignment of anatomical structures, while FREESURFER segmentations and parcellations are based on probabilistic atlases that show better identification of brain structures. To enhance erroneous normalization results, we devised an automated correction heuristic, using the high-quality GM and WM segmentations generated by FREESURFER (Fig. 2) Initially, the heuristic determines which GM voxels of the standard brain image have been erroneously warped onto WM voxels of the subject image and which voxels have been correctly warped onto GM voxels. All MNI voxels that have been falsely warped onto subject-space WM voxels are excluded from the final parcellation, while all MNI parcellation voxels that have been assigned to subject-space GM voxels are assumed to be correct in the final parcellation. Then, the algorithm proceeds by iterating through all unassigned GM voxels and assigning each voxel the label of the majority of GM voxels in its neighborhood. In the case that there are two or more equally sized groups of voxels in the voxel's neighborhood that are assigned to different regions, the search-radius is increased until an unambiguous decision can be made.

Table 1
Computation time and data sizes generated.

CPU clockrate @2.54 GHz					
Suppl. Fig. 1	Data type	Data size	Time/hh:min	Toolbox	Output format
	Raw T1	40 MB			DICOM
	Raw fMRI	270 MB			DICOM
	Raw EEG	85 MB			Brain Vision Analyzer Format
	Raw dw-MRI	110 MB			DICOM
A	Segmentation Parcellation Triangulation	390 MB	9:45	FREESURFER	FREESURFER/Nifti (nii)
B	Preprocessing dMRI	227 MB	00:02	FREESURFER	FREESURFER/Nifti (nii)
C	Transforming the WM/GM interface triangulation into a 3D volume	64 MB	00:00:20	FREESURFER	Nifti (nii)
F	Transforming anatomical masks from individual anatomical to individual diffusion space	69 MB	00:02	FSL	Nifti (nii)
G	Generating WM brain masks for tractography	70 MB	00:02	FSL	Nifti (nii)
H	Computing the fiber Orientation Distribution Function (fODF)	205 MB	00:03	MRTrix	MRTrix image format (mif)
I	Generating seeding-, target- and stop-masks for tracking	40 MB	00:20	MATLAB	MATLAB (mat)/Nifti (nii)
J	Fiber tracking	78 GB	02:00 using 184 CPU cores in parallel	MRTrix	MRTrix track file format (tck)
K	Computing the SC matrices	156 MB	02:00 using 68 CPU cores in parallel	MATLAB	MATLAB (mat)/packed ASCII text files (zip)
L	Region wise aggregation of the BOLD signal	228 MB	01:00	FSL	Nifti (nii)/ASCII (txt)
M	Computing the FC matrix	864 KB	00:00:30	MATLAB	MATLAB (mat)
N	EEG artifact correction			Brain Vision Analyzer	Brain Vision Analyzer Format
P	EEG signal filtering			MATLAB/EEGlab	EEGlab dataset (set)
Q	Lead field matrix computation using Brainstorm	452 MB	01:00	MATLAB/Brainstorm	MATLAB (mat)
R	Converting Brainstorm data into TVB format	9.1 MB	00:02	MATLAB/Brainstorm	ASCII (txt)/packed ASCII (zip)/ MATLAB (mat)
D & E	Normalization to MNI space for including directionality	180 MB	00:45	MATLAB/FSL	Nifti (nii)

Optional: Merging connectomes with directionality information derived from other sources

Directionality of fiber tracks cannot be derived from dwMRI data. However, databases exist that contain directionality information derived from axonal tract-tracing, such as the CoCoMac database (http://cocomac.g-node.org/) that contains several hundreds of published studies. Bezgin et al. (2012) created an approach to register cortical brain regions of macaques and to map them onto a standard macaque brain. The resulting parcellation was warped to the MNI standard human brain template using landmarks defined in Caret (www.nitrc.org/projects/caret) (Van Essen et al., 2001; Van Essen and Dierker, 2007). This mapping between human and monkey brain parcellations enables the merging of directionality information from invasive monkey tracing studies with human structural connectomes. In the pipeline, this merging is realized by warping subject brains onto the MNI152 standard brain, for which the parcellation by Bezgin and colleagues is defined. Connections that were found to be explicitly absent in the macaque brain are deleted from the structural connectomes.

Tractography

Three types of masks are used to constrain tractography and to exclude spurious tracks: seeding-, target- and stop-masks. The GM–WM-interface (GWI) is used as seeding and termination masks for dwMRI-tractography; therefore, FREESURFER's parcellation-masks for the different cortical- and subcortical GM structures are loaded and the WM-voxels adjacent to the structures of interest are defined as seeding- and target-voxels. WM segmentations are used to generate masks that terminate tracks as soon as they leave WM. Since MRTrix and other tractography toolboxes enable sub-voxel tractography, tractography masks are created from FREESURFER's high-resolution parcellations. For this article, we use the Desikan–Killiany atlas (Desikan et al., 2006) as implemented in FREESURFER (excluding the corpus callosum, but including the insular cortices of both hemispheres). The pipeline also enables tracking using FREESURFER's Destrieux atlas, tracking from and to subcortical structures defined by FREESURFER's subcortical segmentation atlas as well as atlases defined for the MNI brain.

Upon extraction of gradient vectors and values (known as b-table) using MRTrix, dwMRI data are pre-processed using FREESURFER's *dt_recon* function. Besides motion correction and eddy current correction (ECC), the b0 image is linearly registered to the subject's anatomical T1-weighted image and the resulting registration rule is used to transform the high-resolution mask volumes from the anatomical space to the subject's diffusion space. Note that there is an ongoing debate over the usefulness of ECC for diffusion data processing (Jones et al., 2013; Soares et al., 2013). A key assumption when performing simple registration based ECC (e.g. via FLIRT's *eddy_correct* algorithm) is that the distortions that are caused by the eddy currents are uniform during the whole scanning time, i.e., over all slices. Hence this assumption does not hold if there is any kind of subject movement during the recording. A more robust approach is to create a time-varying model of distortions caused by eddy currents (Johansen-Berg and Behrens, 2013). Due to the uncertainty about the usefulness of registration-based ECC (e.g., via FSL's *eddy_correct*) its computation is optional in the pipeline.

During MRTrix pre-processing, image-volumes that store the diffusion tensor (i.e., the diffusion ellipsoid) for each voxel are computed. Based on that, a fractional anisotropy (FA) and an eigenvector map are computed and masked by the binary WM mask created previously. For subsequent fiber-response function estimation, a mask containing high-anisotropy voxels (and therefore presumably unidirectional fiber populations) is computed. Probabilistic tractography in MRTrix is based on a constrained spherical deconvolution (CSD) that computes the fiber orientation distribution function (fODF) for each image voxel (Tournier et al., 2004, 2007). For our 64-direction dwMRI data we are able to use a maximum harmonic order of 8.

To address several confounds in the estimation of connection strengths (transmission strengths), tractography is based on a proper selection of seed voxels and on controlling for the number of generated

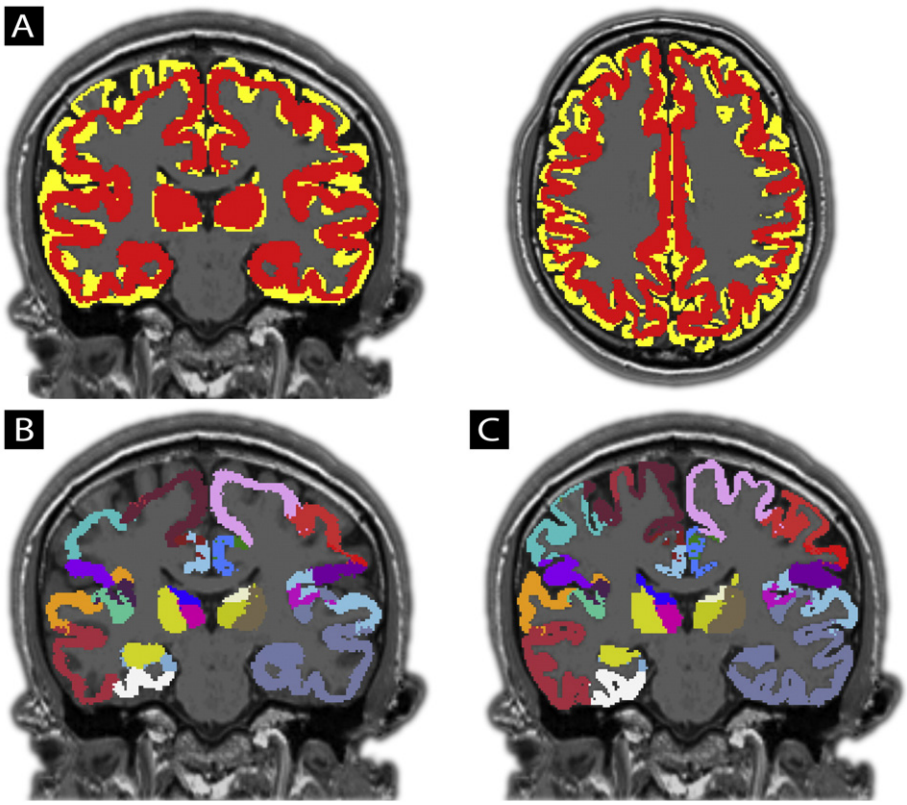

Fig. 2. Nonlinear registration of individual brain anatomy to the MNI152 standard brain can produce strong anatomical mismatches, i.e., anatomical regions are incorrectly mapped: in many cases even parts of GM are registered onto WM and vice-versa. We developed an algorithm that corrects erroneously assigned GM and WM voxels using high-quality FREESURFER segmentations. A) Red indicates GM segmentation obtained by warping the standard brain to the subject's brain; yellow indicates GM as identified by FREESURFER's *recon_all* function. B) GM parcellation before correction. Note the strong deviations from actual anatomy. C) GM parcellation after applying the correction algorithm within the pipeline.

tracks in each seed voxel. To support comparability of resulting connectomes, tracks are initiated from GM–WM-interface voxels instead of using every white matter voxel and a fixed number of tracks are generated for each seed-voxel. Seeding solely from the voxels of the GWI can be problematic due to partial voluming effects and image-noise near the transition between GM and WM. To alleviate this issue, the GWI can be extended into the voxels of the WM, for example by applying mathematical morphology (e.g. dilation).

For parallelization of the computationally intensive tractography part of the pipeline, the seeding mask can be split into several masks each containing only a subset of all GWI voxels allowing multiple instances of MRTrix to perform tractography (all other masks have to contain their full set of voxels). The time needed to complete the whole tractography scales linearly with the number of seeding voxels per mask given enough processors. Along with seeding-masks, target-masks are defined specifying the GWI complement to each seeding region as terminal regions.

During the actual tractography tracks are initiated at uniformly distributed coordinates contained in the seeding ROI and propagated until they reach a termination ROI. All tracks that do not enter the specified termination ROI are discarded. Probabilistic tractography algorithms prolong tracks in a direction that they sample from the fODF of the underlying voxel. The algorithm continues to produce tracks until the specified number of tracks per seed voxel was generated or an upper threshold of tractography attempts is reached (by default this threshold is 1000 times the specified number of wanted tracks). Therefore, the number of tracks that are generated for each region is directly proportional to the size of the GWI of that region. The underlying assumption is that the coupling strength of a region (i.e., the strength of the influence a region can assert over another region) is constrained by the area of the GWI, since it introduces a bottleneck through which the tracks that connect two regions have to pass. By default, a maximum length constraint of 300 mm and a maximum radius of curvature of 1 mm are used. Besides probabilistic tractography the pipeline can also generate tracks using deterministic tractography.

Structural connectome extraction

The connectivity measures derived between each pair of regions are intended to estimate the relative strengths of the influence that regions exert over another, i.e., their SC. Structural connectivity is a relative description of coupling that can be turned into an absolute description of mutual influence that only exists in the context of a specific model and a coupling function that transforms it into effective connectivity (EC) with respect to the specific local node models that are coupled together. However, neither SC nor EC can be directly measured by diffusion imaging and several aspects harden their approximation: First, the diameter of WM fibers is below imaging resolution rendering it impossible to directly resolve actual fiber tracts, but only to concatenate model-based estimations of the diffusion profile at each voxel (i.e., tractography). Second, the impact that a WM tract exerts on a distant neuronal population is dependent on a variety of factors besides the number of axonal connections it contains, e.g., degree of myelination and type, distribution and number of synaptic connections at the terminus of the tract. Third, the number of tracks that was generated for a given pathway does not necessarily reflect the probability of existence or the strength of that pathway. Especially the last problem reflects the confound arising from the dependency of the number of found tracks on path-length and on the shape of the diffusion orientation profile along the pathway due to streamline dispersivity (Liptrot et al., 2014). This issue arises out of the aforementioned problems and

the mechanism of probabilistic tractography: due to step-wise dispersion of the propagating streamline the probability that a specific track is prolonged decreases as a function of the distance from the seed point. This creates a bias towards short pathways and pathways that follow the major diffusion directions. Therefore, the number of found tracks does neither quantify the strength of a connection nor the probability of the existence of a connection but merely reflect the chance that a streamline could propagate along the specific pathway of the tracks. When seeding tractography from every WM-voxel, another bias arises from the fact that tracks that are longer have a higher probability of being tracked than shorter tracks (Jones, 2010; Jbabdi and Johansen-Berg, 2011; Jones et al., 2013; Smith et al., 2013). Figs. 3 and 5 illustrate this multiple-counting bias by comparing raw track counts with the numbers of distinct voxel-to-voxel connections found between two regions. Note the strong multiple counting effect for several connections: for some tractography-runs the raw counts are 40 times larger than the number of distinct voxel-to-voxel connections, i.e., the coupling strength estimated by raw counts is 40 times larger than the relative surface that is used to connect these regions. The right panel of Fig. 5 shows the percentage of all existing connections (thresholded at 1% of maximal unique count value) that has been counted multiple times for different multiples. Note that for about one third of connections of each subject the number of raw counts was at least two times as high as the number of unique connections. Further analyses showed that that the number of multiple counts varies for the same region-to-region connection in different subjects making it unpredictable.

In order to improve existing methods for strength estimation and to address the aforementioned confounds, we make use of several techniques with regard to seed-ROI selection, tractography and aggregation of generated tracks. The basic conjecture behind this approach is that

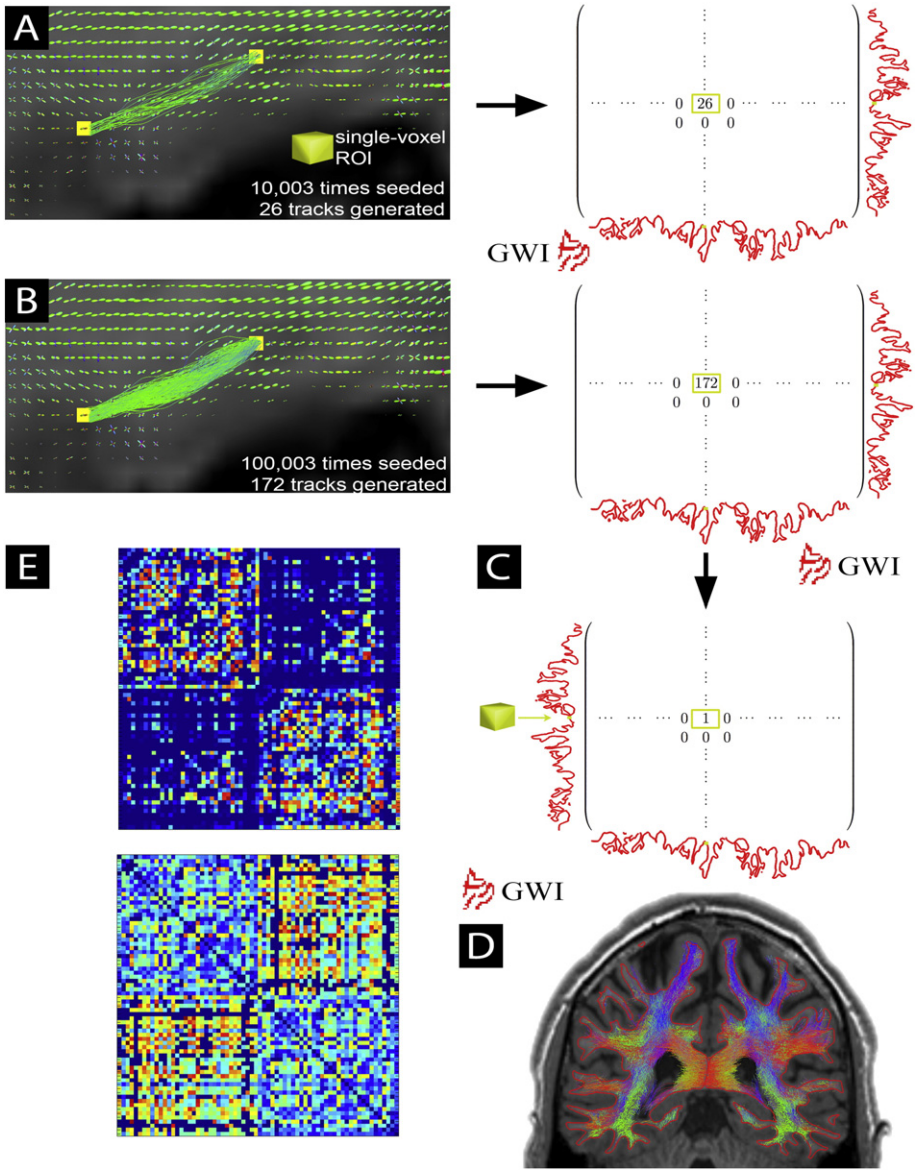

Fig. 3. Strategy for track aggregation using the "bottleneck" assumption. A) Tracks generated between two single voxel ROIs (each 2.3 × 2.3 × 2.3 mm) are shown. Seeding was done at 10,003 uniformly distributed points within the single voxel resulting in 26 valid tracks. Valid tracks produced for each pair of GWI voxels are stored in a matrix (rows, respectively columns contain each voxel of the GWI). B) A ten times higher amount of seed points leads to 172 valid tracks. Note that ten times more seeding attempts do not produce ten times as many valid tracks. C) As a consequence, counting the number of tracks would lead to biased estimates of the connection strength. Therefore, voxel-to-voxel connectomes are binarized prior to region-wise aggregation. D) The GWI, individually segmented and parcellated by FREESURFER for each subject, is used for seeding. E) Voxels of the large matrix are aggregated according to brain regions. Shown are the resulting SC matrices (strengths & distances) from the exemplary subject based on the described algorithm. The rows and columns of the aggregated matrix now do not correspond to single voxels of the interface anymore, but to Atlas regions.

the surface area at both GWI terminals of a tract constrains the number (respectively diameter) of WM fibers that can possibly run between the connected areas and, therefore, constitutes an upper bound to the strength of interaction between these two regions. In other words, the area of the GWI that is used to connect two regions provides a bottleneck to the number of possibly terminating fibers. Thus, we assume that the total surface area on the GWI used to connect two regions limits the strength of that connection. Assuming sufficient homogeneity of cortical microstructure we estimate that the strength of a connection is proportional to the relative surface area that it occupies on the GWI (relative in proportion to the total GWI surface area of a given subject). Based on evidence for cortical microcircuitry invariance (Silberberg et al., 2002; Douglas and Martin, 2004) we use the approximation that each unit of GWI surface area provides an equal amount of coupling strength by restricting the number of axons that can pass through it. In order to connect two GM regions, every tract has to pass through the bottleneck created by the surface area of the GM–WM interface at the terminals of the tracks. We conclude that the maximal coupling strength of all tracks that connect two cortical regions must be bounded by the minimum of the GWI surface areas at both region terminal sites and that consequently the total strength between two regions is proportional to the relative area occupied by tracks.

Since tracks are two-dimensional line objects there is no straightforward way to compute the surface area of a track-terminal. Therefore, we devised a new bundling scheme in order to group tracks into distinct connections. We define a distinct connection as a pair of GWI voxels for which at least one track was generated, regardless of the number of tracks found or the concrete pathway. This metric is further expanded to a second metric by another assumption that states that all distinct connections that share a common terminal voxel must also be bounded by the same bottleneck, and consequently the maximum bandwidth of that voxel must be split up among all distinct connections. Therefore, upon determining all distinct connections for a voxel, the total coupling strength of this voxel is split up over all its distinct connections in equal parts resulting in weighted distinct connections. For example, if a voxel has only one distinct connection with another voxel we assume that the potential coupling strength of that voxel is fully occupied by that single connection. On the other hand, if a voxel has two or more distinct connections we assume that these connections share the possible coupling strength of that voxel. It follows that in this approach the maximal total coupling strength of a region is given by the area of its GWI and not by the amount of tracks that emanate from it, since this number is highly dependent on local anatomy and the characteristics of the diffusion profile. This approach is justified by the assumption that the coupling strength of a region is proportional to the size of the GWI of that region, assuming a fixed ratio of long-range connections per microcircuit volume. We acknowledge that this approximation is the result of several simplifying assumptions on the nature of long-range connectivity that at the moment cannot be verified empirically due to a lack of empirical data. Pseudo-code given in Supplementary material summarizes the steps of the algorithm.

Upon tractography the pipeline computes distinct connections and aggregates them for each region to generate three types of SC matrices (Fig. 3 visualizes details of the concept):

- raw counts, contain track counts of all tracks that were found between each pair of regions (symmetric),
- distinct connection counts, contain only distinct connections between each pair of regions (symmetric),
- weighted distinct connection counts, in which the strength of each distinct connection is divided by the number of all distinct connections leaving the voxel (yielding asymmetric strength matrices).

Each of these metrics is outputted in two variants, namely, absolute values and relative values that have been normalized by the total surface area of the GWI of a subject. Fig. 4A shows the average and inter-subject variance of all resulting coupling strength matrices.

Along with strengths, the pipeline outputs three different SC distances matrices that contain the mean, mode and median lengths of all tracks that were found between each pair of regions. Fig. 4B shows mean SC distances matrices and inter-subject variance of all generated distance SCs. All three weighting schemes for coupling strength estimation follow a similar distribution that approximates a power-law. Matrices are not thresholded, which explains their high density. In separate panels the figure shows the pairwise inter-subject correlation coefficients for all matrix weightings to estimate their similarity.

Test–retest reliability of structural connectome extraction

In order to quantify the robustness of connectome extraction the agreement between SCs of different dwMRI acquisitions of the same subject was contrasted with the agreement of SCs of different subjects. Furthermore, results were compared to the results of similar estimations from other publications. To compare the similarity of SC matrices and to estimate whether inter-subject anatomical variability has a stronger impact on connectome similarity than acquisition noise and estimation biases Pearson's correlation coefficient was computed between all pairwise combinations of matrices. Thereby, matrices of the same strength type were compared between different runs of the same subject (intra-subject variance) but also between scans for different subjects (inter-subject variance). Then, resulting correlation coefficients (CCs) for each type of SC were grouped into intra- and inter-subject CC and visualized by boxplots. Since three subjects have been scanned three times each, this results in three CCs that quantify the pair-wise similarity of matrices for each subject characterizing the intra-subject SC agreement and 27 CCs that characterize inter-subject SC agreement between all three subjects and their three data acquisitions. To further characterize test–retest robustness, the intra-class correlation coefficient, ICC (Shrout and Fleiss, 1979; McGraw and Wong, 1996) was used to assess the degree of consistency among measurements of the same quantity that were made by different observers (multiple scans in our case). ICC(3,1), which was used to estimate consistency in terms of absolute agreement between repeated measurements is computed as

$$\mathrm{ICC}(3,1) = \frac{MC_R - MS_E}{MS_R + (k-1)MS_E}.$$

MS_R denotes the mean square for rows of observations (strengths or distances between nodes and node degrees), MS_E is the mean squared error, k specifies the number of observations and n is the number of scans. ICC(3,1) was computed using the MATLAB method *Intraclass Correlation Coefficient* created by Arash Salarian (www.mathworks.com/matlabcentral/fileexchange/22099). ICC(3,1) estimates the similarity of different strength estimates for the same subject, with a value of 1 indicating perfect agreement between sessions.

In addition to ICCs for full connectivity matrices ICCs for node strengths were computed. The node strength ω_i of node i is defined as the sum of edge weights (i.e., strengths) a_{ij} with all connected nodes j over all n nodes,

$$\omega_i = \sum_{j=1}^{n} a_{ij}.$$

Another type of *Intraclass Correlation Coefficient* was used to specifically test whether global connectivity properties showed larger variability between subjects than within subjects over scanning sessions:

$$\mathrm{ICC} = \frac{\sigma_{bs}^2}{\sigma_{bs}^2 + \sigma_{ws}^2}.$$

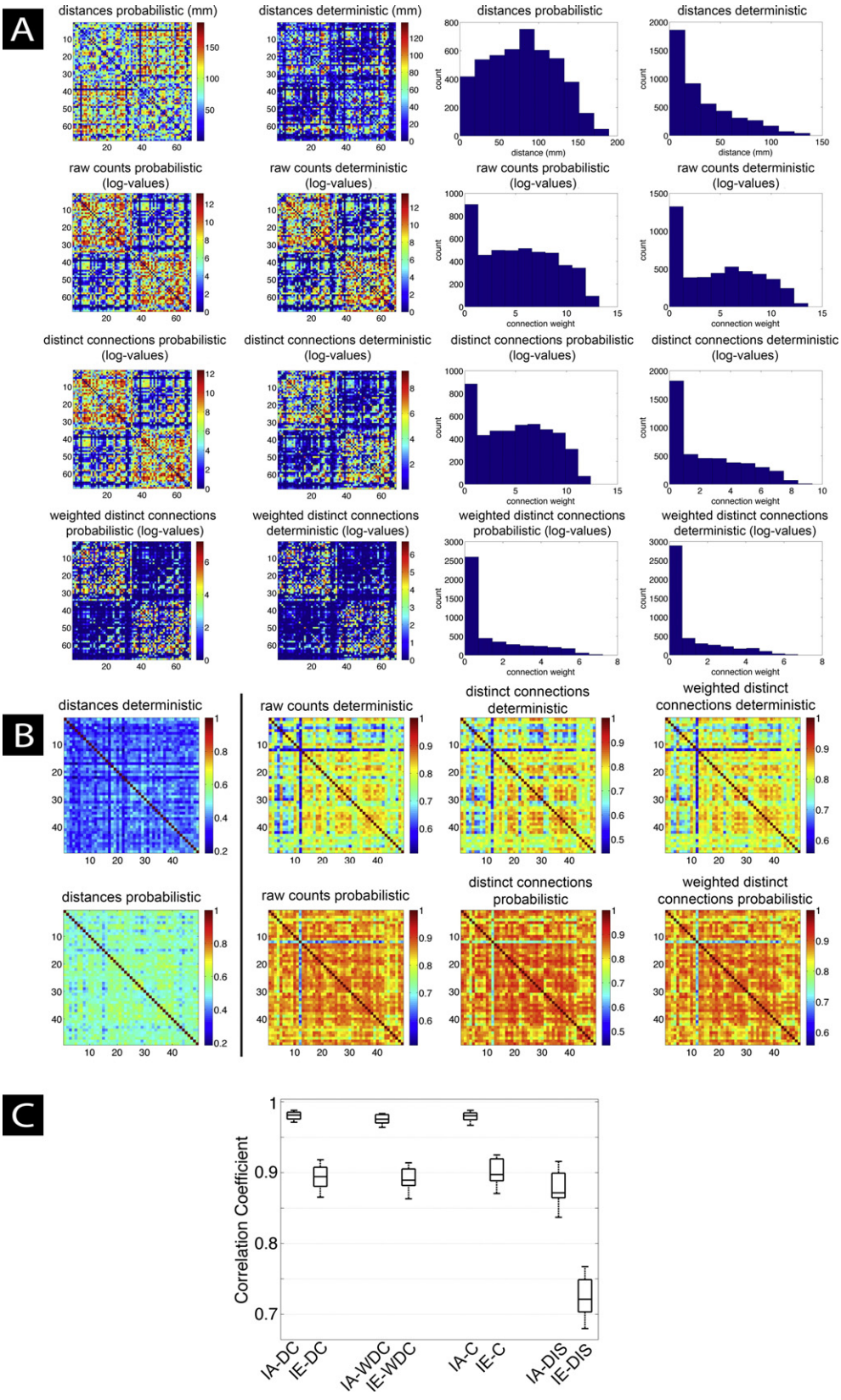

Fig. 4. A) Resulting average SC matrices N = 49 (data sets acquired at Berlin site): distance matrix resulting from probabilistic tractography; distance matrix resulting from deterministic tractography; raw counts matrix resulting from probabilistic tractography; raw counts matrix resulting from deterministic tractography; distinct connection counts matrix resulting from probabilistic tractography; distinct connection counts matrix resulting from deterministic tractography; distinct weighted connection counts matrix resulting from probabilistic tractography; and distinct weighted connection counts matrix resulting from deterministic tractography. B) Correlation coefficients between matrices across all subjects for: Distances probabilistic/deterministic; raw counts probabilistic/deterministic; distinct connection counts probabilistic/deterministic; and distinct weighted connection counts probabilistic/deterministic. C) Intra- compared with inter-subject variability characterized by boxplots of all correlation coefficients (CC) between all pairs of strengths matrices of three subjects and three scans. Boxes labeled with 'IA' denote intra-subject CC, while 'IE' denotes inter-subject CC. DC = distinct connections, WDC = weighted distinct connections, C = raw counts, and DIS = distance.

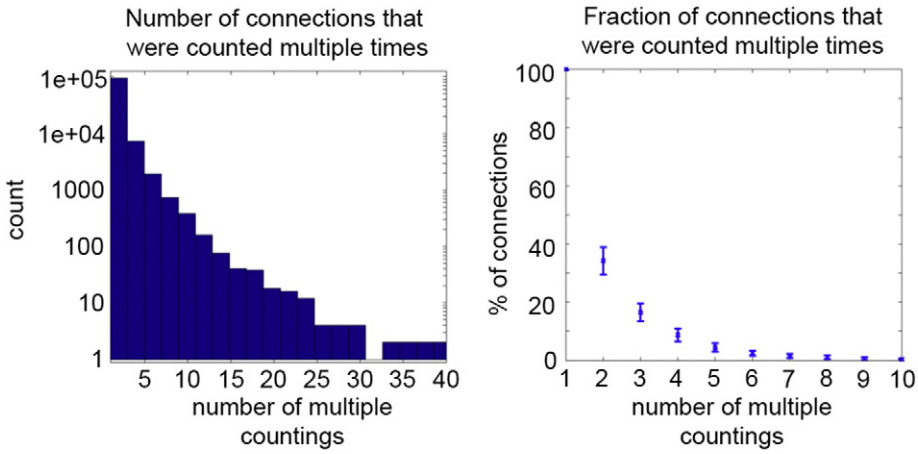

Fig. 5. Illustration of the multiple counting biases. Left panel: Histogram of the pooled ratios between raw track counts and extracted distinct connections (over all subjects). Note that the distribution of multiple count ratios is widespread, indicating strongly heterogeneous ratios of raw counts vs. distinct connections. Right panel: percentage of connections (thresholded at 1% of maximal distinct connections value) that have been counted multiple times. Note that for some subjects almost 40% of connections have been counted at least twice.

Thereby, between-subject variance σ^2_{bs} is contrasted with the pooled within-subject variance σ^2_{ws} of the respective metrics. ICC estimates whether the variability across individuals is lager than the variability present within the estimates for different scans of the same subject. It is a normalized measure that has a maximum of 1; thus, in our application values above 0.5 indicate that there is more variability between subjects than between different scans of the same subject. A complementary measure to characterize the variability of node strengths, the coefficient of variation (CV), was computed. CV is defined as the ratio of the mean within subject standard deviation σ^2_{ws} to the overall measurement mean μ (Lachin, 2004). Variability of node strength was considered low if CV is smaller than 1 and high otherwise.

Fig. 4C compares correlation coefficients obtained by correlating strengths and distances matrices obtained from three data sets of three subjects. All three weighting schemes obtained high CCs (Range, Mean ± Standard Deviation): raw counts (0.97–0.99, 0.98 ± 0.007), distinct connections (0.97–0.99, 0.98 ± 0.006), and weighted distinct connections (0.96–0.98, 0.98 ± 0.007). Inter-subject CCs were considerably lower: raw counts (0.87–0.93, 0.9 ± 0.02), distinct connections (0.87–0.92, 0.89 ± 0.02), and weighted distinct connections (0.86–0.91, 0.89 ± 0.01). Please see Discussion for comparison with published results of others. Distance matrices showed lower intra-subject similarity compared to coupling strength matrices (0.84–0.92, 0.88 ± 0.03). Nevertheless also for the distance metric intra-subject similarity was considerably higher than inter-subject similarity (0.68–0.77, 0.72 ± 0.03). The results of the test–retest analysis using ICC(3,1) are summarized in Table 3. All three strength metrics showed almost perfect within-subject agreement. The agreement of distances, while being lower compared to strength agreement, can still be considered as high. All connectivity properties were computed for the raw unthresholded matrices outputted by the pipeline. Like for overall strength, average ICC(3,1) values for node strength showed almost perfect agreement.

To compare within and between subject variability, population ICC was computed for each node and averaged over all nodes, yielding 0.77 ± 0.16 (distinct connections), 0.76 ± 0.15 (weighted distinct connections) and 0.8 ± 0.13 (raw counts) indicating that there is more variability between subjects than between different scans of the same subject. CVs for node strength were constantly low: 0.07 ± 0.05 (distinct connections), 0.06 ± 0.03 (weighted distinct connections) and 0.05 ± 0.03 (raw counts) indicating that the variability of node strength was low and their estimation robust over different acquisitions.

Functional connectome extraction

In order to generate functional connectivity (FC) matrices, raw fMRI DICOM files are first converted into a single 4D NifTi image file and FSL's FEAT pipeline is used to perform the following operations: deleting the first five images of the series to exclude possible saturation effects, high-pass temporal filtering (100 second high-pass filter), motion correction, brain extraction and a 6 DOF linear registration to the MNI space. Then, BOLD volumes are registered to the subject's T1-weighted images and parcellated according to FREESURFER's cortical segmentation. By inverting the transformation rule found by registration, anatomical segmentations are mapped to the functional space and average BOLD signal time series for each region are generated by computing the temporal mean for all voxel time-series of each region. From the region wise aggregated BOLD data, functional connectivity (FC) matrices are computed within MATLAB using pairwise mutual information (on z-transformed data) and Pearsons's linear correlation coefficient (equations given in Supplementary material). Table 2 shows the correlation between extracted FC and SC matrices.

Discussion

The two essential contributions of this publication are: (i) Provision of an automated pipeline that standardizes the extraction of full-brain network models from neuroimaging data sets and (ii) as part of that pipeline a method for quantitative brain networks extraction that allows for robust transmission strength estimation between brain regions. In the following, we discuss several aspects of multi-modal image processing and connectome extraction and present guidelines and conclusions we drew that lead to standardized connectome extraction and discuss the validity of the approach.

Table 2
Correlation between SC and FC using different tracking methods.

		Deterministic tracking	Probabilistic tracking
Average	Raw counts	0.2192	0.2401
	Distinct connection counts	0.2263	0.2404
	Weighted distinct connection counts	0.2356	0.2503
Averaged matrices	Raw counts	0.3257	0.3395
	Distinct connection counts	0.3390	0.3410
	Weighted distinct connection counts	0.3416	0.3497

Note: For the row "averaged matrices", the average matrices over all 49 subjects where computed and correlated to the average FC of those subjects. Hence this is not the average over all the values in the single columns.

Table 3
Test–retest analysis for pipeline generated SC matrices.

Subject	RC	DC	WDC	DIS	NS(RC)	NS(DC)	NS(WDC)	NS(DIS)
1	0.98	0.98	0.97	0.88	1	1	0.99	0.98
2	0.98	0.98	0.97	0.86	1	0.99	0.99	0.97
3	0.98	0.98	0.98	0.89	1	0.99	0.99	0.98

Summary of test–retest analysis for the three capacities metric and the distance estimation. ICC(3,1) values were computed over full networks with matrices being thresholded at fixed values (thresholds: 4000 for DC, 4500 for RC, 100 for WDC). RC = raw counts, DC = distinct connections, WDC = weighted distinct connections, DIS = distances, and NS = node strength.

Integrating different imaging modalities, file-formats, data-structures and image spaces

In this paper we presented an automated pipeline that extracts full-brain models along with brain activity data ready to import and use within The Virtual Brain. The pipeline automatically extracts information from different imaging modalities such as anatomical-, diffusion-weighted and functional MRI scans as well as simultaneously acquired EEG. The article describes the necessary steps for the robust construction of subject-specific high-quality brain-models, common fallacies that should be avoided, guidelines that improve the quality of connectome extraction and presents a freely available pipeline that integrates all required toolboxes and performs the aggregation of tractography results into one automated processing stream. Different toolboxes often use different image formats and coordinate systems. The raw output files of MRI scanners are often written in the form of DICOM files while image processing software like FSL or SPM typically process analyze or NIfTI volumes. Regarding data structures, raw imaging data is mostly stored as gray-scale images while brain-surface meshes, like those generated with FREESURFER, exist in the form of surface-triangulations specified by coordinates of endpoints and edges that connect them to triangles. Different imaging modalities acquire and store data in different imaging "spaces", e.g., standard atlas space (e.g., Talairach or MNI), structural space (high resolution, small voxel-size), functional space (low to medium resolution, large to medium voxel-size, temporal dimension) or diffusion space (low to medium resolution, large to medium voxel-size, different gradient directions). Images that are defined in the same space can have different resolutions (there exist, e.g., 1 mm and 2 mm isotropic voxel size versions of the MNI152 brain). Images in different spaces need to be registered to each other, that is, the imaged structures must be in spatial alignment in order to operate across modalities (e.g., in the form of masks). To improve spatial resolution high-resolution anatomical images can be used as registration targets and for generating masks for low-resolution images from other modalities. Registration rules are inverted and/or concatenated to transform images or image-related information between spaces. Especially cross-modal registration is an error-prone procedure that complicates standardization making manual intervention necessary. The setting of involved parameters like cost functions, masking, registration parameters (degrees-of-freedom) or quality of brain extraction immensely affect the registration outcome and are often different for different modalities. Besides spatial alignment, temporal alignment is often required when time-series data like EEG, PET or fMRI are simultaneously acquired or are supposed to be processed time-locked to a given event. In the case of simultaneous EEG–fMRI scan markers are written into EEG files in order to synchronize both measurements.

The variety of existing neuroimaging toolboxes, imaging modalities, data-structures, imaging spaces and dimensions along with the amount of degrees of freedom involved in each single processing step and their immense impact on the quality of the analyses calls for a concentration of efforts for standardization of neuroimaging processing streams. While meta-analyses attribute inconsistency in findings to a lack of standardization (Fitzgerald et al., 2006) it is encouraging to see that more and more efforts are being made to overcome this lack: software pipeline scripting tools like Nipype that interface many of the most popular neuroimaging toolboxes or projects like BrainMap (Laird et al., 2011) and protocols like those developed by the 1000 Functional Connectomes Project (Yan et al., 2013) and the Human Connectome Project (Van Essen et al., 2012). What dwMRI still lacks is the acquisition of ground truth data, verification of different tractography approaches and principles and their integration into a single comprehensive framework that is guided by a formalization of a set of best practices.

Standardizing connectome extraction

The proposed method unifies several principles that we consider as mandatory prerequisites for standardization of quantitative large-scale brain network extraction and to compensate for biases arising out of different tractography approaches. In the following, we list several operational considerations and principles for future in-depth discussion and verification. The connectome extraction strategy in the presented pipeline is informed by the conclusions that we draw from the following considerations. Furthermore, they are intended to guide and improve future efforts for robust, reliable and plausible connectome extraction strategies. Tractography is a method that depends on a large number of modeling assumptions and degrees of freedom and its results are determined by the choice of tractography algorithm and parameters involved (Fillard et al., 2011; Bastiani et al., 2012).

Coupling strength estimation

At present, a large and influential part of studies that quantify strengths are estimated by counting all generated tracks between regions (Hagmann et al., 2007, 2008, 2010; Honey et al., 2009). In this regard it is important to acknowledge that tracks estimated by tractography algorithms are model-based approximations of the underlying fiber population, since actual tracts that underlie dwMRI signals are far too small to be resolved by current MR-scanners. For differentiation between the anatomical structure and the theoretical construct a subtle spelling difference has established in current literature: 'tracts' addresses the anatomical structure while 'tracks' labels their tractography based approximation.

Several types of biases interfere with quantification of the strengths of fiber tract reconstructions (Jones, 2010; Jbabdi and Johansen-Berg, 2011; Jones et al., 2013; Smith et al., 2013). Probabilistic connectivity maps are in its most rigorous interpretation nothing more than a map that quantifies the reproducibility of streamline reconstruction of a data set. This is problematic since the probability of tractography for a certain tract does not necessarily depend on its strength but on several other features e.g., it can be shown that "in a set of pathways comprising identical microstructure, the path deemed to mediate the highest connectivity by probabilistic tractography will be the shortest, simplest and straightest path" (Jones, 2010). Since diffusion profiles depend on several different properties of the underlying anatomy, a low tractography count for a certain pathway does neither imply that the underlying tract is thin compared to other tracts, nor, that it has a low coupling strength or even probability of existence, but merely, that it is unlikely to be found by a probabilistic tractography algorithm. Probabilistic tractography provides estimates of the probability that a streamline is found during repeated tractography-runs but not the probability of the existence of a fiber bundle.

The chance for finding a pathway by tractography depends on its shape and diffusion profile: when seeding from all WM voxels, longer and wider tracts will be tracked more often since a higher number of seeds are placed on it. Several approaches (Hagmann et al., 2008; Buchanan et al., 2014) aim to compensate for this by dividing raw tractography counts by the length of the pathway, which introduces a linear weighting to strength estimates that depends on the length of

the tracks. However, the number of found tracks does not only depend on the length and width of the pathway, but on local anatomical features in a highly non-linear manner. One example for local anatomical biases is the dispersion of the ODF profile, which is in probabilistic approaches interpreted as an indicator of crossing fibers. With increasing cumulative dispersion of the ODF along the voxels of a pathway, the probability for the algorithm to branch increases and, consequently, the expected streamline count decreases. Besides structural effects resulting from the underlying anatomy that influence the shape of the ODF it is also highly dependent on several parameters of the MR experiment like b-values, SNR or partial volume effects (Huang et al., 2004).

A conceptual issue arises from the fact that counting tracks (or estimating the thickness of a fiber bundle) is rooted in the idea that the number of axons connecting two regions could be used as an intuitive and straightforward correlate of connection strength. However, the diameter of a fiber tract as well as local anisotropy is not only dependent on the axon count but also depends on several factors like packing, degree of myelination, coherence of axon orientations, membrane permeability and fiber density. Likewise, local anisotropy and thus the ODF are dependent on those features, e.g., lower packing density results in fewer barriers to diffusion. Connectivity strength estimates that are based on the mean anisotropy of a track are similarly biased, i.e., mean anisotropy is highly dependent on the anatomical neighborhood of a track: if the streamline runs through areas that have a relatively homogeneous orientation of fibers, they will also have a high anisotropy and vice versa, regardless of the number of axons. While it is true that anisotropy is modulated by physiological aspects like the degree of myelination, fiber density and packing that certainly affect connectivity strength, it is, however, not possible to disentangle structural effects like incoherent axon orientations, which is the rationale for probabilistic tractography (i.e., spread diffusion profiles as an indicator of crossing fibers).

While hardly any ground truth data exists for coupling strength estimation, the accuracy of tractography algorithms to localize existing major white matter tracts can be verified with a certain amount of confidence (Jbabdi and Johansen-Berg, 2011). Although validation of the topology of extracted connectomes is an active area of research (Seehaus et al., 2013; Schreiber et al., 2014), there is no dataset or method that is able to directly estimate connection strengths between regions for an entire brain. Specifically, the strength of transmission in the sense of a brain network model, as employed by TVB, cannot be directly measured. Furthermore, a method to experimentally probe and disentangle the composite effects of the simultaneous inputs that a region receives does not exist. Note that while increasing efforts investigate the relationship between microstructural properties like axon diameter distribution and diffusion signal (Sherbondy et al., 2010; Pestilli et al., 2014), there is no established relationship between such features and their coupling strength, which is one reason for a strength estimation approach that takes tractography biases into account.

The situation is aggravated by the fact that such connection strengths are only defined in the context of a particular biophysical BNM and therefore no universal unit for strengths exists. In the real scale-free system, connection strengths have a certain physical unit. For example each axon is capable of inducing a certain PSP membrane voltage change in the postsynaptic neuron. Hence candidates are, e.g., voltage change in postsynaptic membranes, mean-field amplitude change, postsynaptic spike-rate, or some quantity of information content. Connection strengths in the present context are expressed as relative quantities that only become functionally interpretable with regard to a specific BNM that turns SC into EC. Local population models like those provided within TVB turn SC into EC by embedding them via population activity models into the interaction infrastructure of a BNM equation that couples local intrinsic dynamics according to the estimated connection strengths. A global coupling-scaling factor rescales the relative SC matrices and turns them into values that assign absolute changes to each simulated population for a unit mean-field change in a connected region.

In order to alleviate the aforementioned issues and to standardize subject-specific connectome extraction we propose several aspects to make the connectome extraction process robust and reliable. Tractography shows good robustness in localizing tracts (Jbabdi and Johansen-Berg, 2011) while, up to now, no dwMRI based metric has been found that allows the direct inference of transmission strengths of reconstructed pathways. Therefore, we opt for uncoupling of strengths estimation from tract reconstruction and to divide connectome estimation into two parts: (i) identification of pathways and (ii) estimation of connection strength. Thereby, we disentangle the quantification of connection strength from the tractography process, which is only used to infer the existence of connections between all GWI voxels without making any assumptions about their strength thus eliminating the multitude of biases arising from track-count based strength estimation.

Morphologically informed coupling strength quantification

In the proposed GWI area normalized approach, quantification of connection strength is based on the assumption that the size of a region (i.e., the number of neurons in a circuit) correlates with the number of outgoing axons. This assumption rests on the notion of a highly conserved and generic cortical microcircuit and a relatively homogeneous connectivity throughout cortex: across many species and regions lamina-specific micro-connectivity structures were found to be variations of a common template (Buxhoeveden and Casanova, 2002; Casanova et al., 2009).

Since we cannot measure the number of outgoing axons of a region, we take the surface area that is used to connect two regions as an indicator of the size of the neural population (and thus outgoing axons). Considering the homogeneous structure of cortical microcircuits we conjecture that large populations have a higher coupling strength than small regions. Furthermore, since each voxel of the WM/GM border can only contain a finite amount of axons (i.e., it constitutes a bottleneck to the number of axons) the maximum coupling strength that can be mediated through a GWI voxel must be bounded from above. For example, if a fiber bundle connects a single voxel from one region to another single voxel from a different region, there is more space for axons to connect these voxels compared to a situation in which the fiber bundle forks and connects to several different voxels. A corollary from this statement is that asymmetric strength matrices are possible in this tractography setup since tracks that occupy a bigger surface area on the GWI of one region can have a greater impact on a connected region where a smaller GWI surface area is occupied. Thus, quantification of connection strength is solely based on the relative surface areas that are occupied by the pathways connecting each region-pair. Tractography is only used to infer the existence of connections, while the estimation of connection strengths depends on the relative surface areas of cortex that are connected. All tracks that connect two given voxels multiple times are aggregated to a single 'unique track'. Each unique track gets either uniform weight or is weighted according to the fraction of unique tracks that are emanating from the two involved voxels resulting in two flavors of connectivity matrices.

The question of whether and to which degree cortical microcircuit invariance exists is a matter of ongoing debate. The notion of widespread existence and homogeneity of ensembles of pyramidal cells surrounded by groups of ~100–200 neurons as basic cortical building blocks, known as minicolumns, enjoys wide support across areas, individuals and species (Silberberg et al., 2002; Douglas and Martin, 2004; Casanova et al., 2009). Nevertheless, the assumptions made in this model are simplifications that might not account for several computationally important aspects, even if homogeneous microcircuitry and bottleneck-like qualities of the GWI are valid approximations for constraining coupling strengths. Neuronal elements that make up basic microcircuits are differentiated into subtypes that vary in occurrence and density in different cortical areas. Variance in cellular and synaptic organization and receptor

distribution lead to considerable functional differences that are not accounted for by the model (DeFelipe et al., 2002). The model also clearly underestimates the eminent importance of sparse modulatory projection systems (e.g., aminergic neurons) for neural computation and also the laminar specificity of long-range tracts (e.g. tracts that target inhibitory interneurons), which will, however, be added in upcoming versions.

Interventional empiric testing allows the generation of effective connectivity maps between remote locations on the basis of cortico-cortical evoked potentials (CCEP) in epileptic patients with subdural electrodes. With this technique distant field potentials are evoked by brief single-pulse electrical stimulation and averaged to compute CCEP maps. Initial results that compare CCEP mapping with anatomical connectivity derived from tractography show a significant positive correlation between the two, essentially showing that pathways with high coupling strengths are more capable of transmitting high amplitude signals (Conner et al., 2011). Since techniques for mapping EC on the basis of brain stimulation are relatively recent developments, no studies exist up to now that relate the size of the stimulation site with evoked potentials at the target site, which would constitute an empirical validation of the employed assumptions. In the absence of such studies, converging evidence can be collected from modeling results that investigate the success of different connectome extraction approaches in predicting functional data in the context of BNM. Correlation of connectomes with phenotypic or other traits can shed light on their biological plausibility, e.g., preliminary partial least square analyses of resulting connectomes showed significant age-depended modulations of several network features (e.g., density of individual axonal tracts ($r = .82$, $p < .01$, 95% CI [0.77, .90]), strength of functional interactions between regions ($r = 0.54$, $p < .01$, 95% CI [0.53, 0.82]) (Zimmermann et al., 2014)).

Choice of seed- and stop-ROIs

In order to compensate for tractography biases on track counts that arise from the size of the ROI and the number of seeds used, we only seed from the GWI, instead of using every WM voxel, which increases the risk for introducing a multiple counting bias. Tractography is done in an exhaustive manner: from every sub-voxel (1 mm isotropic voxel size) multiple tracks are initiated towards a target number of 200 valid tracks, resulting in around 2500 tracks per dwMRI voxel. Seeding from the GWI reduces the effect of the length bias (i.e., longer tracts are more likely to be tracked more often) since tracks are explicitly initiated at the extremities of pathways. While several reasons speak in favor of the GWI as track-termination and seeding site a possible drawback arises from the fact that some reports indicate that a considerable amount of streamlines does not reach the GWI (Hagmann et al., 2007). A further drawback of GWI can result from noise due to imprecise delineation of the GWI and partial volume effects at the overlap zone of GM and WM. Another disadvantageous effect of using the GWI as seeding and target region is a possible bias towards tracks that terminate in gyral crowns since those can be entered straight, while sulcal walls are entered with sharp angles and rejection of corresponding tracks due to angular constraints. While we use the GWI mostly due to the possibility of precise assignment of parcellation labels further improvement could arise from using seeding- and stopping-sites that are buried deeper in WM, although the association of track termination sites with the given gray-matter parcellation would start to blur and become imprecise.

Homogeneous sampling from seeding locations

Another consideration to prevent tractography biases and to standardize tractography approaches is to use a fixed number of tracks that are to be generated instead of a fixed number of seeding attempts in order to ensure homogeneous sampling from seeding locations. During the tractography process a considerable proportion of tracks are rejected due to the violation of tractography constraints. The reasons for track rejection are highly dependent on the individual anatomy of a subject and can even vary within different acquisitions of the same subject due to several reasons like, e.g., scanner noise or partial volume effects. By specifying the number of tracks that the algorithm has to generate it is ensured that an equivalent sampling of WM was attained during different tractography runs to get comparable track counts. In order to make raw track counts comparable across subjects, strengths matrices can be normalized by the number of streamlines used, making connection values independent of the inter-individual differences in size of the GWI.

Another aspect of common tractography approaches that impairs standardized and comparable tractography results is the fact that during many tractography setups seeding masks are used as input that comprise several seeding voxels. Some tractography algorithms will then initialize uniformly distributed seeding locations at subvoxel resolution for each seeding voxel. However, not every seeding attempt will produce a valid track. The number of tracks that are generated for a given amount of attempts varies from voxel to voxel and depends on local anatomical conditions, the form of the fODF and the random numbers that are drawn in each tractography step. Therefore, it is likely that situations arise in which a subset of voxels produced a high number of valid tracks while the remaining voxels only produced intermediate or small numbers of tracks. In order to ensure comparable sampling of seeding locations and to avoid overestimation of connections from a subset of voxels that are more likely to produce valid tracks than other voxel, it is necessary to ensure homogenous sampling from each seeding location.

Test–retest reproducibility

Test–retest robustness of pipeline output and extracted connectomes was demonstrated on a small data set of three subjects with three MRI acquisitions each. In all cases the extracted structural connectomes of the same subjects showed almost perfect agreement and was in general higher than inter-subject similarity indicating that the method is able to infer biologically relevant variability and making it a promising tool for clinical applications.

The principles and standardization guidelines summarized above improve the robustness of connectome extraction since several metrics that quantify reproducibility were higher or at least as high as the highest scores reported in earlier studies. Average intra-subject similarity (mean intra-subject correlation over all weighting schemes: $r = 0.98$, ICC(3,1) >0.97) was highest compared to earlier approaches while maintaining between-subject variability (mean inter-subject correlation over all weighting schemes: $r = 0.89$): Hagmann et al. (2008) found a correlation of $r = 0.78$ for connectomes extracted from repeated scans of the same subject, Cheng et al. (2012) yielded mean correlations of 0.89 ± 0.046 and 0.84 ± 0.07 for two different weighting schemes. Cammoun et al. (2012) scanned five subjects twice and obtained for a 83-regions parcellation an average correlation of 0.98, however inter-subject correlation was almost on the same scale ranging between 0.94 and 0.96, which might indicate hampered inference of biological variability. Besson et al. (2014) used a surface-based tractography approach and defined node weights as the number of fibers per unit area. They report inter-acquisition correlations of connection strengths of 0.81 ± 0.03, node degree correlations of 0.91 ± 0.05 and CV of node degrees <1 (except for 0.26% of surface triangles) across 10 acquisitions from a single subject. Buchanan et al. (2014) computed a variety of strength estimates obtaining a maximal mean ICC(3,1) value of 0.76 for global network strength and 0.62 for node strength. Bassett et al. (2011a) also quantified similarity between connectivity matrices using correlation coefficients and found comparable values for intra- and inter-subject similarity. Variability in connectome estimates are most likely to be attributed to the accumulation small variations in each processing step in

particular the error-prone steps atlas segmentation and cross-modal registration.

Limitations in terms of accuracy of the presented pipeline depend on the quality of the involved several image-processing streams. Accuracy of cortical and subcortical segmentations and white-matter surface reconstructions by FREESURFER are crucial for correct seeding and results aggregation of tractography. Cross-modal registration between anatomical- and diffusion-weighted images is a highly error prone step and likely subject to failure or imprecision when preceding brain extraction steps fail and visual verification of registration results is crucial. The test–retest data set (three subjects, acquired three times) was small and is only used as a preliminary evaluation of rescan reliability. Especially for computing reliable estimates of intraclass-correlation coefficients sample size was too small. Buchanan et al. (2014) recommend for future dwMRI connectome studies to use a sample of more than 50 subjects. Another limitation arises from the fact that cortical and subcortical segmentation and regionalization is based on anatomical features of GM and parcellates it into relatively large chunks. While coarse parcellations may augment resilience to image- and processing noise, they may also hamper the extraction of genuine structural differences between subjects, especially when recognizing that macroscopic landmarks (folding pattern of sulci and gyri) are not necessarily a good indicator for localization of functional units and that, conversely, extrinsic connectivity of a cortical area determines its functionality (Jbabdi and Johansen-Berg, 2011).

While we could clearly demonstrate the precision (reproducibility of the result) of the approach we are still not able to quantify its accuracy (proximity of estimated to true value) due to a lack of ground truth data. Up to now we can only rely on the converging evidence resulting from modeling studies that predict brain dynamics on the basis of such structural connectomes like it is done within the framework of TVB. Other constraints (beyond biological reality and precision) are imposed by the simulation environments such as TVB, which require certain accuracy in spatial precision of the network, as well as the time delays of the reconstructed fiber tracks. So far no systematic computational studies exist that could shed light on the required parameter ranges beyond more qualitative proof of concept studies (Jirsa and Stefanescu, 2011).

Source imaging

Several choices can be made during source imaging that require careful consideration with regard to the underlying (M)EEG data and the intended purpose of the estimated source time-series. Brainstorm offers a variety of options and source imaging algorithms that impact the resulting source time-series. Regarding head model computation, three models are available in Brainstorm: The simpler single sphere and overlapping sphere models (approximating the head as spheres) and the more advanced BEM included from the open-source software OpenMEEG. While the simpler models deliver proper results for MEG, for EEG the BEM model should be preferred, especially if subject specific anatomical data is available. Noise covariance estimation is sensitive with regard to the type of EEG experiment done and the intended use of the data. Source reconstruction requires an estimation of the noise that is present in different sensors. For MEG, sensor noise can be estimated by recording the activity present in the sensors while the scanning room is empty. For EEG, however, it is not easily possible to disentangle noise from signal since the noise level depends primarily on the quality of the connection with the skin. Even worse, noise tends to be non-stationary due to movement of the cap or drying out of the electrode gel. For stimulation experiments a resting baseline or a pre-stimulation baseline can be used for estimating noise. However, for resting-state data like that used in this article this is not possible since meaningful activity can be subtracted this way. As a remedy, noise can be estimated by computing it over a long segment of resting data and to save only the diagonal of the matrix, i.e., the variance of the sensors, like it was done in this case. If noise modeling is renounced, it is possible that electrodes with high noise levels are interpreted as high activity in its corresponding regions of the brain. Several source estimation approaches have been developed and some of them are implemented in Brainstorm. For brain modeling purposes within the scope of this article sLORETA (Pascual-Marqui, 2002) was chosen since it estimates current densities with zero localization error which is preferred when comparing highly localized simulated brain activity with empirical activity. Regarding the variety of choices that can be made during source imaging, it is advisable to not fully automate the source estimation process, but to consider the impact each step has on the resulting data with respect to their intended use.

Supplementary data to this article can be found online at http://dx.doi.org/10.1016/j.neuroimage.2015.03.055.

Acknowledgments

The authors acknowledge the support of the German Ministry of Education and Research (Bernstein Focus State Dependencies of Learning 01GQ0971) to PR, the James S. McDonnell Foundation (Brain Network Recovery Group JSMF22002082) to ARM, VJ, PR, and the Max Planck Society (Minerva Program) to PR.

References

Akil, H., Martone, M.E., Van Essen, D.C., 2011. Challenges and opportunities in mining neuroscience data. Science 331 (6018), 708–712.

Allen, E.A., Damaraju, E., Plis, S.M., Erhardt, E.B., Eichele, T., Calhoun, V.D., 2014. Tracking whole-brain connectivity dynamics in the resting state. Cereb. Cortex 24 (3), 663–676. http://dx.doi.org/10.1093/cercor/bhs352.

Bassett, D.S., Brown, J.A., Deshpande, V., Carlson, J.M., Grafton, S.T., 2011a. Conserved and variable architecture of human white matter connectivity. NeuroImage 54 (2), 1262–1279.

Bassett, D.S., Wymbs, N.F., Porter, M.A., Mucha, P.J., Carlson, J.M., Grafton, S.T., 2011b. Dynamic reconfiguration of human brain networks during learning. Proc. Natl. Acad. Sci. 108 (18), 7641–7646.

Bastiani, M., Shah, N.J., Goebel, R., Roebroeck, A., 2012. Human cortical connectome reconstruction from diffusion weighted MRI: the effect of tractography algorithm. NeuroImage 62 (3), 1732–1749.

Besson, P., Lopes, R., Leclerc, X., Derambure, P., Tyvaert, L., 2014. Intra-subject reliability of the high-resolution whole-brain structural connectome. NeuroImage 102 (2), 283–293.

Bezgin, G., Vakorin, V.A., van Opstal, A.J., McIntosh, A.R., Bakker, R., 2012. Hundreds of brain maps in one atlas: registering coordinate-independent primate neuroanatomical data to a standard brain. NeuroImage 62 (1), 67–76.

Biswal, B.B., Mennes, M., Zuo, X.N., Gohel, S., Kelly, C., Smith, S.M., Beckmann, C.F., Adelstein, J.S., Buckner, R.L., Colcombe, S., Dogonowski, A.M., Ernst, M., Fair, D., Hampson, M., Hoptman, M.J., Hyde, J.S., Kiviniemi, V.J., Kotter, R., Li, S.J., Lin, C.P., Lowe, M.J., Mackay, C., Madden, D.J., Madsen, K.H., Margulies, D.S., Mayberg, H.S., McMahon, K., Monk, C.S., Mostofsky, S.H., Nagel, B.J., Pekar, J.J., Peltier, S.J., Petersen, S.E., Riedl, V., Rombouts, S.A., Rypma, B., Schlaggar, B.L., Schmidt, S., Seidler, R.D., Siegle, G.J., Sorg, C., Teng, G.J., Veijola, J., Villringer, A., Walter, M., Wang, L., Weng, X.C., Whitfield-Gabrieli, S., Williamson, P., Windischberger, C., Zang, Y.F., Zhang, H.Y., Castellanos, F.X., Milham, M.P., 2010. Toward discovery science of human brain function. Proc. Natl. Acad. Sci. U. S. A. 107 (10), 4734–4739.

Buchanan, C.R., Pernet, C.R., Gorgolewski, K.J., Storkey, A.J., Bastin, M.E., 2014. Test–retest reliability of structural brain networks from diffusion MRI. NeuroImage 86, 231–243.

Bullmore, E., Sporns, O., 2009. Complex brain networks: graph theoretical analysis of structural and functional systems. Nat. Rev. Neurosci. 10 (3), 186–198.

Buxhoeveden, D.P., Casanova, M.F., 2002. The minicolumn hypothesis in neuroscience. Brain 125 (5), 935–951.

Calhoun, V.D., Lemieux, L., 2014. Neuroimage: special issue on multimodal data fusion. NeuroImage 102 (1), 1–2.

Cammoun, L., Gigandet, X., Meskaldji, D., Thiran, J.P., Sporns, O., Do, K.Q., Maeder, P., Meuli, R., Hagmann, P., 2012. Mapping the human connectome at multiple scales with diffusion spectrum MRI. J. Neurosci. Methods 203 (2), 386–397.

Casanova, M.F., Trippe, I., Tillquist, C., Switala, A.E., 2009. Morphometric variability of minicolumns in the striate cortex of Homo sapiens, Macaca mulatta, and Pan troglodytes. J. Anat. 214 (2), 226–234.

Cheng, H., Wang, Y., Sheng, J., Kronenberger, W.G., Mathews, V.P., Hummer, T.A., Saykin, A.J., 2012. Characteristics and variability of structural networks derived from diffusion tensor imaging. NeuroImage 61 (4), 1153–1164.

Conner, C.R., Ellmore, T.M., DiSano, M.A., Pieters, T.A., Potter, A.W., Tandon, N., 2011. Anatomic and electro-physiologic connectivity of the language system: a combined DTI-CCEP study. Comput. Biol. Med. 41 (12), 1100–1109.

Craddock, R.C., Jbabdi, S., Yan, C.G., Vogelstein, J.T., Castellanos, F.X., Di Martino, A., Kelly, C., Heberlein, K., Colcombe, S., Milham, M.P., 2013. Imaging human connectomes at the macroscale. Nat. Methods 10 (6), 524–539.

DeFelipe, J., Alonso-Nanclares, L., Arellano, J.I., 2002. Microstructure of the neocortex: comparative aspects. J. Neurocytol. 31 (3–5), 299–316.

Desikan, R.S., Ségonne, F., Fischl, B., Quinn, B.T., Dickerson, B.C., Blacker, D., Buckner, R.L., Dale, A.M., Maguire, R.P., Hyman, B.T., 2006. An automated labeling system for subdividing the human cerebral cortex on MRI scans into gyral based regions of interest. NeuroImage 31 (3), 968–980.
Douglas, R.J., Martin, K.A., 2004. Neuronal circuits of the neocortex. Annu. Rev. Neurosci. 27, 419–451.
Fillard, P., Descoteaux, M., Goh, A., Gouttard, S., Jeurissen, B., Malcolm, J., Ramirez-Manzanares, A., Reisert, M., Sakaie, K., Tensaouti, F., 2011. Quantitative evaluation of 10 tractography algorithms on a realistic diffusion MR phantom. NeuroImage 56 (1), 220–234.
Fitzgerald, P.B., Oxley, T.J., Laird, A.R., Kulkarni, J., Egan, G.F., Daskalakis, Z.J., 2006. An analysis of functional neuroimaging studies of dorsolateral prefrontal cortical activity in depression. Psychiatry Res. 148 (1), 33–45.
Friston, K.J., Harrison, L., Penny, W., 2003. Dynamic causal modelling. NeuroImage 19 (4), 1273–1302.
Grabner, G., Janke, A.L., Budge, M.M., Smith, D., Pruessner, J., Collins, D.L., 2006. Symmetric atlasing and model based segmentation: an application to the hippocampus in older adults. Medical Image Computing and Computer-Assisted Intervention—MICCAI. Springer, pp. 58–66.
Hagmann, P., Cammoun, L., Gigandet, X., Gerhard, S., Grant, P.E., Wedeen, V., Meuli, R., Thiran, J.P., Honey, C.J., Sporns, O., 2010. MR connectomics: principles and challenges. J. Neurosci. Methods 194 (1), 34–45.
Hagmann, P., Cammoun, L., Gigandet, X., Meuli, R., Honey, C.J., Wedeen, V.J., Sporns, O., 2008. Mapping the structural core of human cerebral cortex. PLoS Biol. 6 (7), e159.
Hagmann, P., Kurant, M., Gigandet, X., Thiran, P., Wedeen, V.J., Meuli, R., Thiran, J.P., 2007. Mapping human whole-brain structural networks with diffusion MRI. PLoS One 2 (7), e597.
Honey, C.J., Sporns, O., Cammoun, L., Gigandet, X., Thiran, J.P., Meuli, R., Hagmann, P., 2009. Predicting human resting-state functional connectivity from structural connectivity. Proc. Natl. Acad. Sci. U. S. A. 106 (6), 2035–2040.
Huang, H., Zhang, J., van Zijl, P.C., Mori, S., 2004. Analysis of noise effects on DTI-based tractography using the brute-force and multi-ROI approach. Magn. Reson. Med. 52 (3), 559–565.
Hutchison, R.M., Womelsdorf, T., Allen, E.A., Bandettini, P.A., Calhoun, V.D., Corbetta, M., Della Penna, S., Duyn, J.H., Glover, G.H., Gonzalez-Castillo, J., 2013. Dynamic functional connectivity: promise, issues, and interpretations. NeuroImage 80, 360–378.
James, A.P., Dasarathy, B.V., 2014. Medical image fusion: a survey of the state of the art. Inf. Fusion 19, 4–19.
Jbabdi, S., Johansen-Berg, H., 2011. Tractography: where do we go from here? Brain Connect. 1 (3), 169–183.
Jirsa, V.K., Jantzen, K.J., Fuchs, A., Kelso, J.A., 2002. Spatiotemporal forward solution of the EEG and MEG using network modeling. IEEE Trans. Med. Imaging 21 (5), 493–504.
Jirsa, V.K., Sporns, O., Breakspear, M., Deco, G., McIntosh, A.R., 2010. Towards the virtual brain: network modeling of the intact and the damaged brain. Arch. Ital. Biol. 148 (3), 189–205.
Jirsa, V.K., Stefanescu, R.A., 2011. Neural population modes capture biologically realistic large scale network dynamics. Bull. Math. Biol. 73 (2), 325–343.
Johansen-Berg, H., Behrens, T.E.J., 2013. Diffusion MRI: From Quantitative Measurement to In vivo Neuroanatomy. Academic Press.
Jones, D.K., 2010. Challenges and limitations of quantifying brain connectivity in vivo with diffusion MRI. Imaging Med. 2 (3), 341–355.
Jones, D.K., Knösche, T.R., Turner, R., 2013. White matter integrity, fiber count, and other fallacies: the do's and don'ts of diffusion MRI. NeuroImage 73, 239–254.
Jorge, J., Van Der Zwaag, W., Figueiredo, P., 2014. EEG–fMRI integration for the study of human brain function. NeuroImage 102 (1), 24–34.
Lachin, J.M., 2004. The role of measurement reliability in clinical trials. Clin. Trials 1 (6), 553–566.
Laird, A.R., Eickhoff, S.B., Fox, P.M., Uecker, A.M., Ray, K.L., Saenz, J.J., McKay, D.R., Bzdok, D., Laird, R.W., Robinson, J.L., 2011. The BrainMap strategy for standardization, sharing, and meta-analysis of neuroimaging data. BMC Res. Notes 4 (1), 349.
Liptrot, M.G., Sidaros, K., Dyrby, T.B., 2014. Addressing the path-length-dependency confound in white matter tract segmentation. PLoS One 9 (5), e96247.
Marcus, D.S., Olsen, T.R., Ramaratnam, M., Buckner, R.L., 2007. The Extensible Neuroimaging Archive Toolkit: an informatics platform for managing, exploring, and sharing neuroimaging data. Neuroinformatics 5 (1), 11–34.
McGraw, K.O., Wong, S.P., 1996. Forming inferences about some intraclass correlation coefficients. Psychol. Methods 1 (1), 30.
Pascual-Marqui, R., 2002. Standardized low-resolution brain electromagnetic tomography (sLORETA): technical details. Methods Find. Exp. Clin. Pharmacol. 24 (Suppl. D), 5–12.
Pestilli, F., Yeatman, J.D., Rokem, A., Kay, K.N., Wandell, B.A., 2014. Evaluation and statistical inference for human connectomes. Nat. Methods 11 (10), 1058–1063.
Ritter, P., Schirner, M., McIntosh, A.R., Jirsa, V.K., 2013. The virtual brain integrates computational modeling and multimodal neuroimaging. Brain Connect. 3 (2), 121–145.
Roy, D., Sigala, R., Breakspear, M., McIntosh, A.R., Jirsa, V.K., Deco, G., Ritter, P., 2014. Using the virtual brain to reveal the role of oscillations and plasticity in shaping brain's dynamical landscape. Brain Connect. 4 (10), 791–811.
Sanz-Leon, P., Knock, S.A., Spiegler, A., Jirsa, V.K., 2015. Mathematical framework for large-scale brain network modelling in The Virtual Brain. NeuroImage 111, 385–430.
Sanz-Leon, P., Knock, S.A., Woodman, M.M., Domide, L., Mersmann, J., McIntosh, A.R., Jirsa, V., 2013. The Virtual Brain: a simulator of primate brain network dynamics. Front. Neuroinf. 7.
Schreiber, J., Riffert, T., Anwander, A., Knösche, T.R., 2014. Plausibility tracking: a method to evaluate anatomical connectivity and microstructural properties along fiber pathways. NeuroImage 90, 163–178.
Seehaus, A.K., Roebroeck, A., Chiry, O., Kim, D.-S., Ronen, I., Bratzke, H., Goebel, R., Galuske, R.A., 2013. Histological validation of DW-MRI tractography in human postmortem tissue. Cereb. Cortex 23 (2), 442–450. http://dx.doi.org/10.1093/cercor/bhs036.
Sherbondy, A.J., Rowe, M.C., Alexander, D.C., 2010. MicroTrack: an algorithm for concurrent projectome and microstructure estimation. Medical Image Computing and Computer-Assisted Intervention—MICCAI 2010. Springer, pp. 183–190.
Shrout, P.E., Fleiss, J.L., 1979. Intraclass correlations: uses in assessing rater reliability. Psychol. Bull. 86 (2), 420.
Silberberg, G., Gupta, A., Markram, H., 2002. Stereotypy in neocortical microcircuits. Trends Neurosci. 25 (5), 227–230.
Sivagnanam, S., Majumdar, A., Yoshimoto, K., Astakhov, V., Bandrowski, A., Martone, M.E., Carnevale, N.T., 2013. Introducing the Neuroscience Gateway. IWSG, Citeseer.
Smith, R.E., Tournier, J.D., Calamante, F., Connelly, A., 2013. SIFT: spherical-deconvolution informed filtering of tractograms. NeuroImage 67, 298–312.
Soares, J.M., Marques, P., Alves, V., Sousa, N., 2013. A hitchhiker's guide to diffusion tensor imaging. Front. Neurosci. 7, 31.
Sporns, O., 2013. Making sense of brain network data. Nat. Methods 10 (6), 491–493.
Sporns, O., Tononi, G., Kotter, R., 2005. The human connectome: a structural description of the human brain. PLoS Comput. Biol. 1 (4), e42.
Tournier, J.D., Calamante, F., Connelly, A., 2007. Robust determination of the fibre orientation distribution in diffusion MRI: non-negativity constrained super-resolved spherical deconvolution. NeuroImage 35 (4), 1459–1472.
Tournier, J.D., Calamante, F., Gadian, D.G., Connelly, A., 2004. Direct estimation of the fiber orientation density function from diffusion-weighted MRI data using spherical deconvolution. NeuroImage 23 (3), 1176–1185.
Uludağ, K., Roebroeck, A., 2014. General overview on the merits of multimodal neuroimaging data fusion. NeuroImage 102 (1), 3–10.
Valdes-Sosa, P.A., Roebroeck, A., Daunizeau, J., Friston, K., 2011. Effective connectivity: influence, causality and biophysical modeling. NeuroImage 58 (2), 339–361.
Van Essen, D.C., Dierker, D.L., 2007. Surface-based and probabilistic atlases of primate cerebral cortex. Neuron 56 (2), 209–225.
Van Essen, D.C., Drury, H.A., Dickson, J., Harwell, J., Hanlon, D., Anderson, C.H., 2001. An integrated software suite for surface-based analyses of cerebral cortex. J. Am. Med. Inform. Assoc. 8 (5), 443–459.
Van Essen, D.C., Ugurbil, K., Auerbach, E., Barch, D., Behrens, T.E., Bucholz, R., Chang, A., Chen, L., Corbetta, M., Curtiss, S.W., Della Penna, S., Feinberg, D., Glasser, M.F., Harel, N., Heath, A.C., Larson-Prior, L., Marcus, D., Michalareas, G., Moeller, S., Oostenveld, R., Petersen, S.E., Prior, F., Schlaggar, B.L., Smith, S.M., Snyder, A.Z., Xu, J., Yacoub, E., Consortium, W.U.-M.H., 2012. The Human Connectome Project: a data acquisition perspective. NeuroImage 62 (4), 2222–2231.
Woodman, M.M., Pezard, L., Domide, L., Knock, S.A., Sanz-Leon, P., Mersmann, J., McIntosh, A.R., Jirsa, V., 2014. Integrating neuroinformatics tools in TheVirtualBrain. Front. Neuroinf. 8.
Yan, C.-G., Craddock, R.C., Zuo, X.-N., Zang, Y.-F., Milham, M.P., 2013. Standardizing the intrinsic brain: towards robust measurement of inter-individual variation in 1000 functional connectomes. NeuroImage 80, 246–262.
Zalesky, A., Fornito, A., Cocchi, L., Gollo, L.L., Breakspear, M., 2014. Time-resolved resting-state brain networks. Proc. Natl. Acad. Sci. 111 (28), 10341–10346.
Zimmermann, J., McIntosh, A.R., Ritter, P., Rothmeier, S., Schirner, M., 2014. Structural architecture supports local and global functional interactions in healthy aging. Poster PresentationSociety for Neuroscience.